T. R. Knutson · R. E. Tuleya

Increased hurricane intensities with CO$_2$-induced warming as simulated using the GFDL hurricane prediction system

Abstract The impact of CO$_2$-induced global warming on the intensities of strong hurricanes is investigated using the GFDL regional high-resolution hurricane prediction system. The large-scale initial conditions and boundary conditions for the regional model experiments, including SSTs, are derived from control and transient CO$_2$ increase experiments with the GFDL R30-resolution global coupled climate model. In a case study approach, 51 northwest Pacific storm cases derived from the global model under present-day climate conditions are simulated with the regional model, along with 51 storm cases for high CO$_2$ conditions. For each case, the regional model is integrated forward for five days without ocean coupling. The high CO$_2$ storms, with SSTs warmer by about 2.2 °C on average and higher environmental convective available potential energy (CAPE), are more intense than the control storms by about 3–7 m/s (5%–11%) for surface wind speed and 7 to 24 hPa for central surface pressure. The simulated intensity increases are statistically significant according to most of the statistical tests conducted and are robust to changes in storm initialization methods. Near-storm precipitation is 28% greater in the high CO$_2$ sample. In terms of storm tracks, the high CO$_2$ sample is quite similar to the control. The mean radius of hurricane force winds is 2 to 3% greater for the composite high CO$_2$ storm than for the control, and the high CO$_2$ storms penetrate slightly higher into the upper troposphere. More idealized experiments were also performed in which an initial storm disturbance was embedded in highly simplified flow fields using time mean temperature and moisture conditions from the global climate model. These idealized experiments support the case study results and suggest that, in terms of thermodynamic influences, the results for the NW Pacific basin are qualitatively applicable to other tropical storm basins.

1 Introduction

Greenhouse gas-induced climate warming could potentially affect hurricanes in a number of important ways, including intensity, frequency or location of occurrence, storm size, tracks, rainfall amounts, and so forth. Studies of possible changes in storm frequency/location changes have been attempted using global climate models (Broccoli and Manabe 1990; Haarsma et al. 1993; Bengtsson et al. 1996; Krishnamurti et al. 1998; Royer et al. 1998) with variable results. In this study, we examine primarily the question of possible CO$_2$-induced changes in hurricane intensities. Recent assessments of this issue include Kattenberg et al. (1996) who concluded in the 1995 Intergovernmental Panel on Climate Change (IPCC) report that "…it is not possible to say whether the … maximum intensity of tropical cyclones will change" due to increased greenhouse gas concentrations; and Henderson-Sellers et al. (1998) who conclude that "… the MPI (maximum potential intensity) of cyclones will remain the same or undergo a modest increase …" in response to doubled CO$_2$.

Observational studies of hurricane intensities (Merrill 1988; Evans 1993; DeMaria and Kaplan 1994a; Whitney and Hobgood 1997; Baik and Paek 1998; Kuroda et al. 1998) suggest an increase in the upper limit intensities of tropical cyclones with increasing SST. However, such an empirical SST/intensity relationship cannot be reliably extrapolated to the question of hurricane intensity changes under CO$_2$-induced warming, since other environmental factors, such as wind shear, lapse rates (Holland 1997), and large-scale regions of ascent and descent, may also change regionally in various ways. In terms of historical trends, Henderson-Sellers et al. (1998) report no clear evidence

T. R. Knutson (✉) · R. E. Tuleya
Geophysical Fluid Dynamics Laboratory/NOAA,
PO Box 308, Princeton, New Jersey 08542, USA
e-mail: tk@gfdl.gov

for long-term trends in storm intensities for the north Atlantic and western North Pacific, although Landsea et al. (1996) noted an apparent *decrease* in the occurrence of intense Atlantic hurricane in recent decades.

Theoretical models of hurricane intensity predict that the MPI of hurricanes will increase in a warmer climate (Emanuel 1987; Henderson-Sellers et al. 1998) based on thermodynamical considerations. Since the MPI theories contain assumptions and caveats (Emanuel 1986, 1988, 1995a; Holland 1997; Henderson-Sellers et al. 1998) it is important to test their conclusions using alternative methods. Rotunno and Emanuel (1987) have shown that MPI theory agrees well with simulation results from a convection-resolving non-hydrostatic axisymmetric model; here we use a hydrostatic, three-dimensional hurricane model to investigate the sensitivity of hurricane intensities to CO_2-induced changes in large-scale environmental conditions.

Although global climate models could in principle be used directly to examine both thermodynamical and dynamical (e.g., shear, storm interaction) influences on storm intensities, unfortunately the resolution of the models used to date for CO_2-induced climate change studies has been too coarse to allow a simulation of realistic hurricane structure or of the most intense storms. For example, Bengtsson et al. (1995) report that even using a T106 global model (grid resolution of 1.1°) the lowest central surface pressure simulated was 957 hPa. This is much weaker than the observed record low central pressure of 870 hPa, the 906 hPa storm simulated in Hamilton and Hemler's (1997) exploratory 1/3° resolution global model simulation, or the 849 hPa minimum pressure simulated for one of the control storms in the present study. Thus, the reliability of global models used to date to address possible climate-related intensity changes has been questioned (Henderson-Sellers et al. 1998 and references therein). Nonetheless, some global climate models have provided suggestive, though not highly convincing, indications of increased hurricane intensities in a warmer climate (Haarsma et al. 1993, Krishnamurti et al. 1998).

Regional models have a long history in explorations of the influence of SST on storm intensities (e.g., Ooyama 1969; Tuleya and Kurihara 1982; Evans et al. 1994), although these early studies mostly involved altering only SST and without changes to the atmospheric temperature profile. This contrasts with the MPI methods mentioned, which either explicitly (Holland 1997) or implicitly (Emanuel 1986, 1988, 1995a) incorporate enhanced warming of the upper troposphere, relative to lower levels, with increased SST. Drury and Evans' (1993) numerical experiments explored the impact on hurricane intensity of increasing SST under different atmospheric temperature change conditions. Although their study was limited to a few cases, they found that the degree of SST-induced storm intensification was considerably reduced if atmospheric temperatures were adjusted in such a way that convective available potential energy (CAPE) was unchanged in the warm SST scenario.

Recently, Knutson et al. (1998) used a three-dimensional high resolution regional hurricane model with boundary conditions from a global climate model to study of hurricane intensity/climate relationships. The simulated NW Pacific typhoon intensities in these experiments increased by 5–12% for an SST warming of 2.2 °C. Here we expand on this study, examining possible CO_2-induced changes in storm structure, storm precipitation, and mean storm tracks for the NW Pacific basin. We also examine CO_2-induced changes in the large-scale environmental conditions from the global climate model; explore the relationship between storm intensities and several environmental measures (e.g., CAPE, vertical wind shear); and test the robustness of CO_2-induced intensity changes to modifications of the storm initialization procedure. In addition, we use an idealized model framework to explore the effect of CO_2-induced environmental changes on storm intensities in each of the major tropical storm basins.

2 Methodology

In our case study approach, 51 tropical storm cases were selected from a control simulation of a global climate model and 51 cases from a high CO_2 simulation. Each case was then integrated for five-days using a regional high-resolution hurricane forecast system, and the statistics of the resulting storms compared. The cases were selected from the northwest tropical Pacific region, where the strongest tropical cyclones are observed in the present climate. The simulated tropical storm frequency climatology in the R30 global climate model (to be reported in detail elsewhere, see also Broccoli and Manabe 1992) is more realistic in the NW Pacific than in other basins, (e.g., the NW Atlantic and NE Pacific) which discourages our use of the case study technique in those basins. For our more idealized experiments (described in more detail in Sect. 5), the hurricane forecast system was used with temporally and spatially averaged environmental fields derived from the climate model for each of the major tropical storm basins.

2.1 Global climate model

The global model used is the GFDL R30 coupled ocean-atmosphere climate model (Manabe et al. 1991; Knutson and Manabe 1998). The atmosphere has resolution of about 2.25° latitude (250 km) by 3.75° longitude (400 km) and 14 vertical finite difference (σ = pressure/surface pressure) levels. The spectral domain representation of variables has rhomboidal truncation at wave number 30 (i.e., R30). Tropical storm-like features (weaker and much broader than observed) have previously been analyzed by Broccoli and Manabe (1990) for an R30 global atmospheric model very similar to that used here. The ocean model is an 18-level finite difference global ocean GCM (Modular Ocean Model, version 1) with a top layer thickness of 32 m, and with the same latitudinal resolution and twice the longitudinal resolution as the atmospheric model. The coupled model uses a flux adjustment technique for heat and salinity fluxes at the ocean surface to reduce model drift (Manabe et al. 1991). Two 120-y experiments were done with the model (Knutson and Manabe 1998): a control integration with CO_2 constant at present day levels,

and an idealized transient CO_2 increase experiment in which atmospheric CO_2 levels increased at $+1\%/yr$ compounded throughout the experiment (that is, by factors of 2.0, 2.57, and 3.3 by years 70, 95, and 120, respectively).

2.2 Storm case selection

Storm cases were selected from a fairly small region of the northwest Pacific basin ($8°-26°N$, $124°-161°E$) which we will show results in similar track statistics for our control and high CO_2 samples. Fifty-one storm cases (one per year) were selected from years 70–120 of the control experiment and 51 cases from years 70–120 of the CO_2 increase experiment. The cases selected were GCM storms with surface wind speeds of at least 17.5 m/s, strong cyclonic surface flow, and an upper tropospheric warm core structure (see Appendix for further details).

2.3 Regional hurricane model

For the regional model experiments, the GFDL Hurricane Prediction System (Kurihara et al. 1998) was used. This system, currently used operationally at the US National Centers for Environmental Prediction (NCEP), consists of an 18-level hydrostatic triply nested-moveable-mesh atmospheric model with a model-generated initial vortex. The outer grid covers a $75° \times 75°$ region at a resolution of $1°$, while the inner-most grid covers a $5° \times 5°$ region at a resolution of $1/6°$, or about 18 km. This model provides for a significantly stronger and more compact representation of hurricanes, and in that sense is more realistic than the global climate model. In addition to spatial resolution, the global and regional models differ in model physics, diurnal variation, etc. The SSTs, which were held fixed during the regional "forecast" experiments, and the initial environmental conditions for each case were derived from the global climate model. We note that the climate sensitivity of a hypothetical global version of the hurricane model could be different from that of the R30 global climate model, but is not investigated here. The various model differences, such as spatial resolution, physics, etc., can be expected to lead to differences between the regional and global model climatologies. Thus the environmental fields in the regional model will tend to adjust toward the regional model's climatology during the five-day integrations. In our study, since these adjustments occur in both the control and high CO_2 cases, it is assumed that their net effect on the *sensitivity* results (high CO_2 minus control) is small compared to the CO_2-induced changes in intensity.
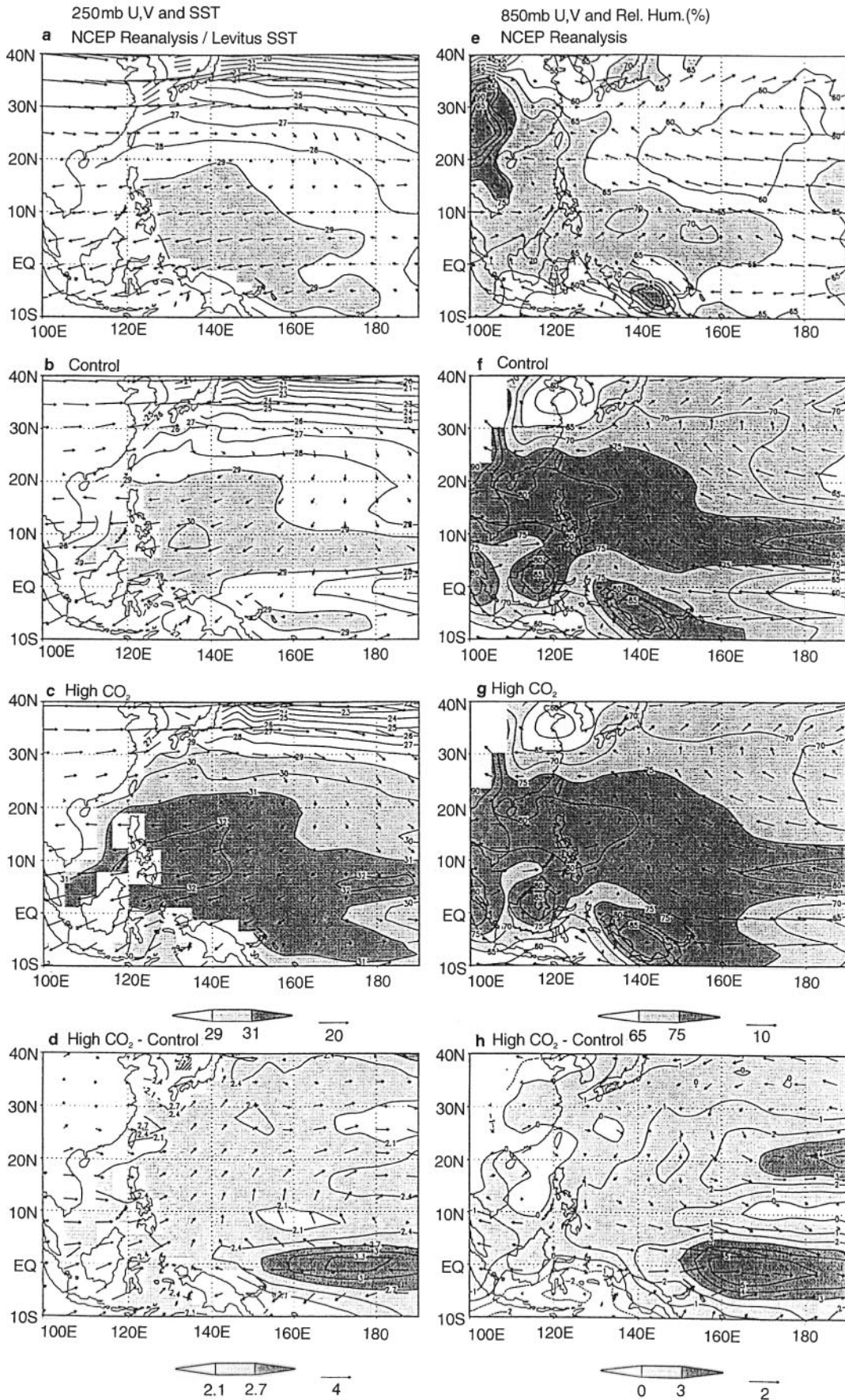
2.4 Initialization procedure

Before each hurricane model simulation, the crudely resolved global model storm (but not the background environment) was filtered from the global model fields and replaced by a more realistic vortex generated with the GFDL hurricane model's initialization scheme (Kurihara et al. 1993). This generated disturbance field was combined with the background environmental fields to create the regional model's initial condition for the five-day integration. This procedure is analogous to that presently used operationally for hurricane prediction at NCEP, except that in the operational case the disturbance target is based on actual storm estimates and the global fields are derived from operational analyses. For our base study, an initial disturbance target wind speed of 17.5 m/s and radius of maximum wind of 175 km were specified for each of the case studies. Except as noted in the text, results shown are for this "standard bogus" specification. Sensitivity tests using different initial condition specifications are described in Sect. 4.

3 Global model tropical climatology

In this section, the global climate model's tropical climatology is briefly compared with observed climatologies and with the high CO_2 run, with particular emphasis on the NW Pacific region. The comparisons with observations are based on 1979–1995 NCEP reanalysis data (Kalnay et al. 1996) for winds and relative humidity (RH) and on SSTs from Levitus (1982). Figure 1 shows the July to November mean conditions for the NW Pacific. The control run SST is slightly warmer than observed over parts of the warm pool (Fig. 1b versus 1a), but the overall regional SST simulation is fairly similar to the observed as expected from the use of flux adjustment in the coupled model. The 250 hPa and 850 hPa winds (Fig. 1b, f) broadly resemble the NCEP data (Fig. 1a, e), although the simulated equatorial easterlies at 850 hPa are too strong in association with an over-developed equatorial cold tongue in the model (Fig. 1b). The simulated 850 hPa relative humidity is systematically higher by roughly 10% than the NCEP reanalysis over most of the region (Fig. 1e, f). With increased CO_2, a fairly uniform warming of over $2°C$ is simulated in the region (Fig. 1d), but with a pronounced local maximum in warming centered on the equator just west of the dateline (see Knutson and Manabe 1998). Associated with this equatorial SST warming maximum are slightly weaker 850 hPa easterlies within about 10 degrees of the equator (Fig. 1f–h); and an anticyclonic flow anomaly at 250 hPa just north of the equator in the high CO_2 minus Control difference field (Fig. 1d). The 850 hPa relative humidity is slightly higher in the high CO_2 run (Fig. 1h) over most of the study region, with the changes generally of the order of a 1–2%; an increase of about 5% is simulated near the maximum equatorial SST warming.

Comparisons of the vertical profiles of the mean zonal wind are shown in Fig. 2 for the NW Pacific and NW Atlantic basins. The broad-scale features of the NCEP reanalysis data are represented in the climate model simulation. For example, both the climate model and NCEP data show a deep layer of weak easterly flow in the NW Pacific and substantial vertical shear of the zonal wind in the NW Atlantic. The upper tropospheric westerlies in the NW Atlantic maximize at a lower level in the climate model than in the NCEP data. The general features of the simulated zonal wind profiles are not dramatically altered between the control and high CO_2 climates. In fact the CO_2-induced changes are generally smaller than the differences between the control run and the NCEP data. A slight enhancement of the vertical shear in the NW Atlantic is apparent in the high CO_2 simulation, relative to the control; this feature will be examined further in Sect. 5.

Vertical profiles of CO_2-induced air temperature change for various tropical basins are shown in Fig. 3a. In each of the basins, the warming is distinctly larger in

250mb U,V and SST

a NCEP Reanalysis / Levitus SST

850mb U,V and Rel. Hum.(%)

e NCEP Reanalysis

b Control

f Control

c High CO_2

g High CO_2

d High CO_2 - Control
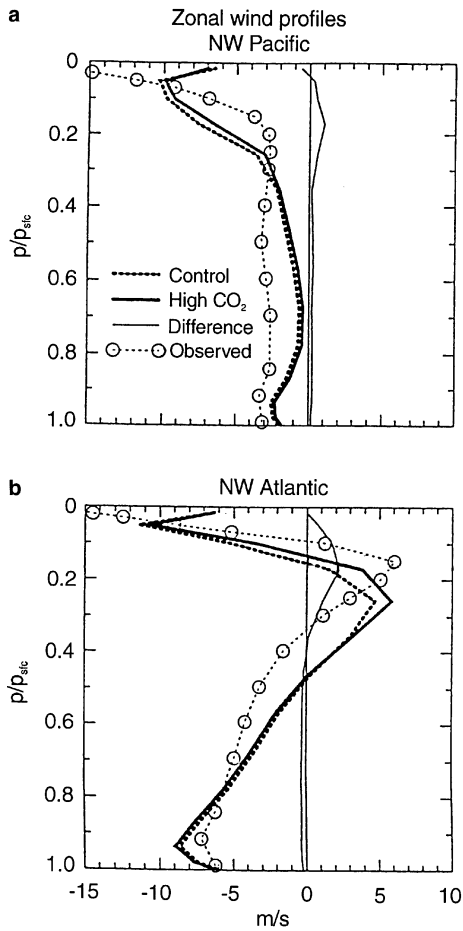
h High CO_2 - Control

Fig. 2a, b Vertical profiles of area-averaged zonal wind for the **a** NW Pacific and **b** NW Atlantic basins. In each diagram, averages are shown for the control run for years 71–120 (*dark dashed*); high CO_2 run for years 71–120 (*dark solid*); high CO_2 minus control (*light solid*); and NCEP Reanalysis for 1979–1995 (*light dashed with circles*). The regions are defined as follows: NW Pacific: July–November; 124°–161 °E, 8°–26 °N; NW Atlantic: July–November; 49°–79 °W, 10°–26 °N.
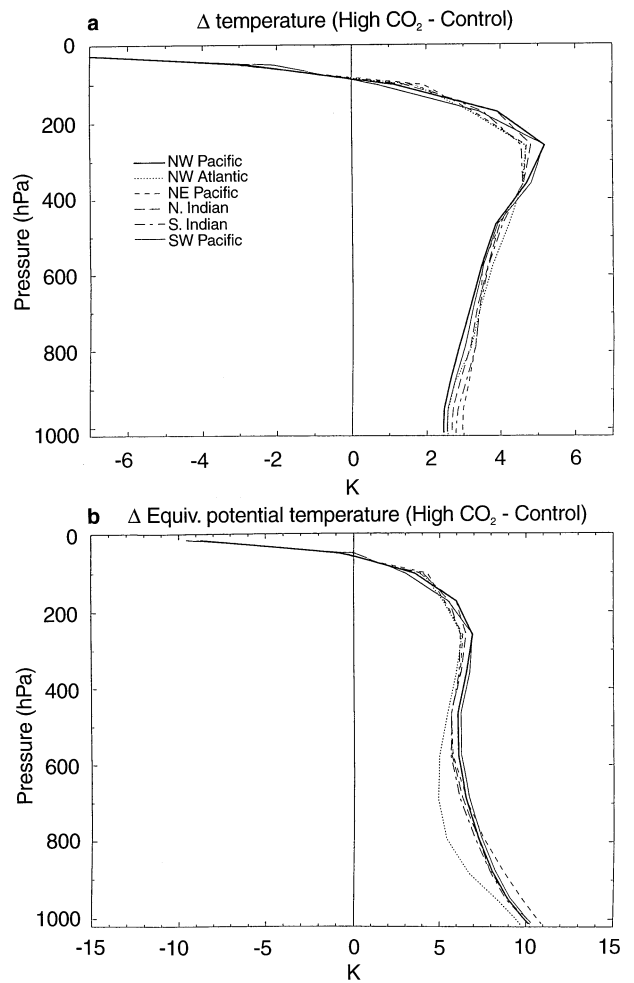
◄──────────────

Fig. 1a–h Observed (**a, e**), control run (**b, f**), and high CO_2 run (**c, g**) climatologies for July through November; and high CO_2 minus control difference fields (**d, h**). Model data are for years 71–120 of the R30 coupled model control and + 1%/y CO_2 experiments. The contoured *shaded fields* are SST (°C) in the *left column* (**a–d**) and 850 hPa relative humidity in the *right column* (**e–h**). The vector fields are wind speeds (m/s) at 250 hPa (**a–d**) and 850 hPa (**e–h**). A *reference vector* is shown below each diagram

the upper troposphere (> 5 °C) than near the surface. For example, in the NW Pacific (dark line) the warming exceeds 5 °C in the upper troposphere compared with less than 2.5 °C near the surface. This enhanced upper tropospheric warming is a consequence of fact that the model's vertical lapse rate remains close to moist

Fig. 3a, b Vertical profiles of CO_2-induced changes in **a** temperature and **b** equivalent potential temperature (θ_e) in Kelvin for the R30 coupled model based on years 71–120 of the control and + 1%/y CO_2 experiments. The region definitions are as follows: NE Pacific: July–November; 101°–131 °W, 10°–19 °N; N. Indian: May–June, September–December; 64°–94 °E, 8°–19 °N; SW Pacific: December–March; 150 °E–150 °W, 8 °S–19 °S; S. Indian: December–March; 60 °–120 °E, 8 °S–19 °S. See Fig. 2 caption for NW Pacific and NW Atlantic basin definitions

adiabatic in the tropics resulting in larger temperature increases in the upper troposphere than near the surface in a warmer climate. The CO_2-induced change in equivalent potential temperature (θ_e) for each basin is shown in Fig. 3b. Despite the enhanced warming of the upper troposphere (Fig. 3a), θ_e increases more in the lower troposphere than in the upper troposphere due to the pronounced increase of moisture at lower levels, implying an increase in moist instability. The CAPE, computed assuming pseudoadiabatic ascent for an air parcel lifted from the lowest global model level ($\sigma = 0.997$) was 16% higher for the high CO_2 conditions. An increase of CAPE in the warmer climate is consistent with the CAPE theories of Renno and Ingersoll (1996) and Emanuel and Bister (1996).

A caveat to the results in the present study is that they are based on CO_2-induced changes as simulated by the GFDL global climate model only. While climate models generally indicate a greater warming in the upper troposphere than near the surface, the models show somewhat conflicting projections of CO_2-induced changes in the vertical gradient of θ_e, (e.g., Henderson-Sellers et al. 1998, Fig. 5b; Bengtsson et al. 1996). In addition, Cunningham and Mitchell (1990) found that the vertical profile of CO_2-induced air temperature warming in their model was sensitive to the convective parametrization used.

Estimates of the vertical profile of zonal mean tropospheric temperature changes in the tropics since the 1960 s derived from radiosonde observations (e.g., Karoly et al. 1994; Tett et al. 1996) show less warming in the upper troposphere than near the surface, somewhat at variance with GCM simulations using various radiative forcings. However, questions remain, for example, concerning the reliability of the radiosonde data for assessing long-term trends (Gaffen 1994; Hansen et al. 1997; Luers and Eskridge 1998).

4 Hurricane model case studies

4.1 Storm tracks

The storm tracks from the hurricane model for each of the 51 five-day simulations are shown in Fig. 4a and b for the control and high CO_2 conditions, respectively. No systematic differences between the control and high CO_2 samples are apparent in the figure. The mean tracks for these samples are shown by the dark curves in Fig. 5a. The mean track for the high CO_2 cases has a slightly more poleward trajectory than the control, although the two mean tracks are rather similar overall. The mean tracks for the respective storms from the climate model (light curves Fig. 5a) are also rather similar between Control and high CO_2 conditions. Note that the time-mean climate model fields in Figs. 1 and 2 indicate that the changes in winds are relatively small in the region just east of the Philippines and southeast of Japan where the case studies are located.

Comparison of the control run mean tracks for the global model and regional model (Fig. 5a) indicates that the global model storms have a distinctly more poleward trajectory; this is also apparent for the high CO_2 mean tracks. Based on the barotropic nondivergent vortex motion studies of DeMaria (1985) and Fiorino and Elsberry (1989) we speculate that the more poleward trajectory of the global model storms is due primarily to their much larger size in comparison to the hurricane model storms. As a further exploration of the track differences, Fig. 5b shows the mean track from a sensitivity study for the 51 control cases without use of the bogusing technique (Sect. 2.4); the mean control
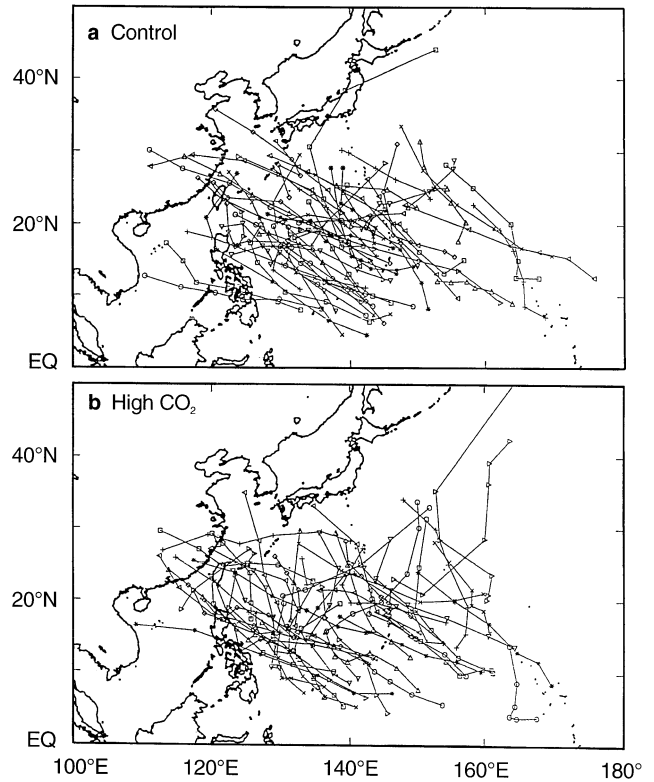

Fig. 4a, b Storm tracks (position every 24 h) for **a** the 51 control and **b** 51 high CO_2 case studies as simulated using the regional hurricane model

run tracks from the hurricane model and climate model are also shown (reproduced from Fig. 5a). The "no bogus" cases begin with much larger (climate model scale) disturbances than the bogus cases, but tend to become more compact and intense during the five-day regional simulation (not shown). Consistent with this, the mean track for the "no bogus" cases is close to that of the climate model cases during the first 24 h, but approaches the hurricane model "bogus" cases mean track during the final three days.

4.2 Storm intensities

4.2.1 High CO_2 versus control case studies

A comparison of the distribution of maximum wind speeds (one value per storm) for the control and high CO_2 case studies is shown in Fig. 6b. The high CO_2 distribution is shifted toward higher intensities by roughly 5 m/s. The median of the wind speed distribution is 3.2 m/s higher for the high CO_2 than for the control, and the median central surface pressure (not shown) is 6.6 hPa lower (i.e., more intense). The Kolmogorov-Smirnov (KS) one-sided two-sample test (Siegel and Castellan 1988) is used to test whether
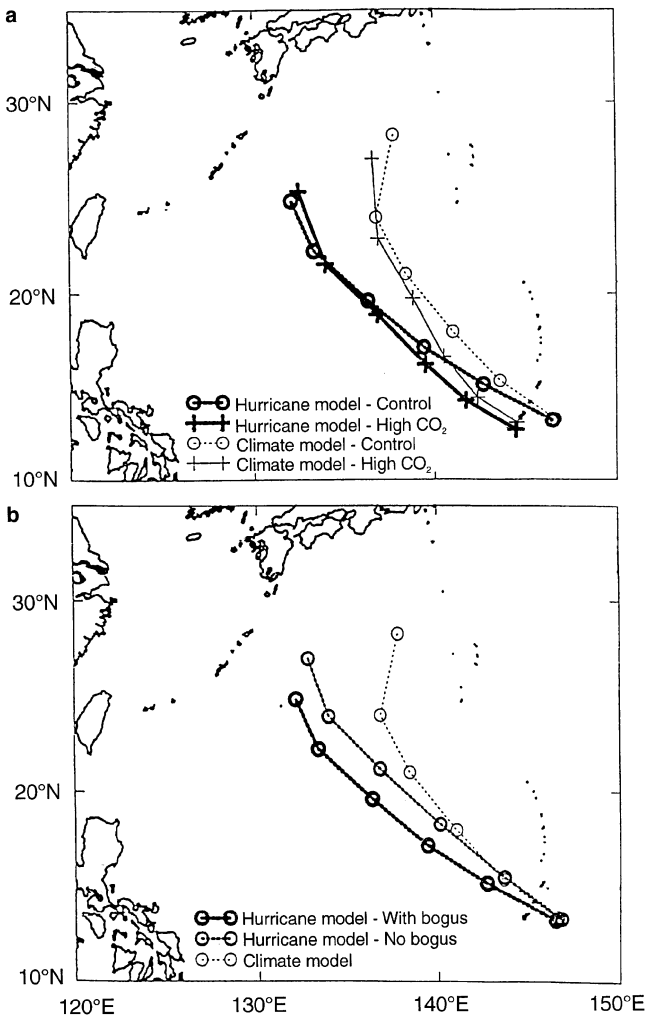
a

b

Fig. 5 a Mean storm tracks (based on 24-h positions) for the 51 control (o's) and 51 high CO_2 (+ 's) case studies. *Dark* and *light lines* show the mean tracks for the regional hurricane model and global climate model simulations, respectively. **b** As in **a** but for control conditions only; the *dark dashed line* is based on hurricane model cases without use of the bogusing procedure for the initial disturbance
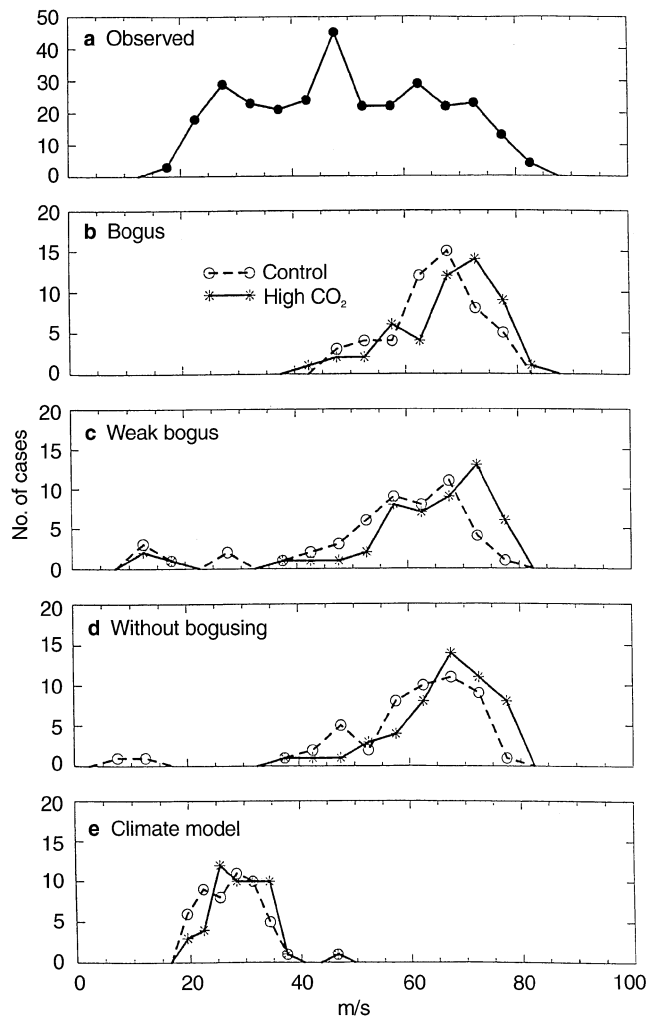
Fig 6a–e Observed **a** or simulated **b–e** frequency distribution of maximum surface wind speeds (one per storm) in the NW Pacific basin. Observations in **a** are from the Joint Typhoon Warning Center (Guam). See text for further details. Simulated distributions in **b–d** are from the regional model, and in **e** from the global climate model. Dashed and solid lines in **b–e** correspond to control and high CO_2 experiments. The initial storm disturbances in **b–d** were specified as follows: **b** bogus vortex with maximum wind speed of 17.5 m/s and radius of maximum wind of 175 km; **c** bogus vortex with maximum wind speed of 10 m/s, radius of maximum wind of 25 km, and relatively shallow vertical depth; **d** no bogusing – initial disturbance taken from global climate model

values in one sample are statistically larger (or smaller) than those of a second independent sample based upon the cumulative distributions. This test indicates that the tendency for the high CO_2 storms in Fig. 6b to have more intense surface winds than the control storms is statistically significant at the 90% confidence level, with a probability of obtaining such a result by chance (p_{KS}) of 0.059. The high CO_2 storms are taken from a range of years (70–120) during which the model's climate continues to warm. The maximum intensities of these high CO_2 cases have a positive trend of 6.0 m/s/100 y although the trend is not statistically significant. Comparing the minimum central surface pressures (high CO_2 versus control cases) the CO_2-induced intensification was not significant ($p_{KS} = 0.20$) according to the KS test, although six of the seven

strongest storms in terms of central pressure are high CO_2 cases (Knutson et al. 1998, Fig. 3). The lowest central pressure among the high CO_2 cases was 834 hPa compared with 849 hPa for the control cases.

The maximum wind speeds for the *global climate model* storms (two 51-case samples) are compared in Fig. 6e. Note that the global model storms are generally much weaker than the regional model storms. The high CO_2 climate model cases were slightly more intense than the control cases, but the difference is not statistically significant according to the KS test ($p_{KS} = 0.28$).

The sensitivity of our case study results to the use of the bogus initial vortex is shown in Fig. 6d. This diagram is based on a set of experiments like that in Fig. 6b, but using the climate model fields (without storm removal and bogus vortex insertion) as initial conditions for the regional model. These "no bogus" results (Fig. 6d) are quite similar to the bogus case (Fig. 6b) with a slightly higher intensity for the high CO_2 storms relative to the control, although for the "no bogus" cases the intensity changes are more statistically significant. The median of the maximum wind speed values was 4.1 m/s (7%) higher, with $p_{KS} = 0.036$ for the KS test. The median surface pressure was 11.2 hPa lower, with $p_{KS} = 0.012$.

The top panel (Fig. 6a) shows a distribution of observed maximum storm intensities (one value per storm) for the NW Pacific basin. The observed data in Fig. 6a are from the Joint Typhoon Warning Center (Guam) as compiled by C.J. Neumann as of 1993 and were obtained from NCAR (http://www.scd.ucar.edu.dss). The data period analyzed was 1971 to 1992 for the months of July to November and within the region $8°–26°N$, $124°–161°E$ to match our study region. The storms shown each had a reported intensity of at least 17.5 m/s for at least four (6-hourly) observations while located within the study region. The distribution of maximum reported intensities for such storms (Fig. 6a) has a much broader distribution than the intensity distribution of the storms simulated by the regional model. The high-intensity end of the simulated distribution is in reasonable agreement with the observed high-end, but there are relatively few occurrences of lower intensity storms (e.g., less than 40 m/s) in the simulated distribution.

The reasons for the lack of weak simulated storms are not entirely clear. One possibility which we have examined is whether the specified initial vortex is so robust (moderately high initial wind speeds of 17.5 m/s at a rather large radius of maximum wind of 175 km), as to lead to fairly intense storms in all cases. To test such a possibility, we repeated the case studies with a much weaker initial disturbance (10 m/s, 25 km radius of maximum wind, and a shallower vertical depth). The results in Fig. 6c show a few more occurrences of weaker storms than with the stronger bogus cases (Fig. 6b), but with an overall distribution still skewed toward strong storms. The CO_2-induced intensification "signal" is more pronounced in the weak bogus comparison (Fig. 6c) than in the strong bogus comparison (Fig. 6b). For the weak bogus cases, the median intensity is 6.6 m/s (11%) higher for the high CO_2 sample, and for the KS test $p_{KS} = 0.0064$; for surface pressure, the median was 24 hPa lower, with $p_{KS} = 0.0033$. A second possible reason for the lack of weak storms is that our storm case selection procedure, by emphasizing relatively strong and long-lived climate model storm cases (Appendix), preferentially selects unusually favorable environments (e.g., low shear) for storm intensifi-

cation. A third possible reason is the lack of ocean coupling in the regional model. Both model studies and observations (see Bender et al. 1993 and references therein) indicate that tropical cyclones can induce an SST cooling of several degrees in the vicinity of a storm, and thus lead to a reduction in the storm intensity compared to the case of no ocean coupling. Other possibilities include the regional model's tendency to over-develop weak systems (Kurihara et al. 1998), or possibly that the large-scale environments from the climate model are overly conducive to development in the hurricane model.

The potential biases introduced by the possibilities mentioned are present for both control and CO_2 case studies, whereas our sensitivity study emphasizes the systematic *differences between* the control and CO_2 case study ensembles. Nonetheless, the hurricane model sample appears to be most representative of the intensity of the strongest storms in the region, rather than of the overall distribution of storm intensities.

4.2.2 Environmental influences on storm intensity

In this section we analyze the case studies to explore the influence of various environmental factors on storm intensity in the model. The distribution of maximum storm intensities versus in situ SST was shown in Knutson et al. (1998) for the control and high CO_2 case studies. In Fig. 7 are scatter plots of simulated maximum intensities in the hurricane model versus several other environmental measures believed to be related to storm intensity, including the environmental CAPE (e.g., Williams and Renno 1993), and maximum potential intensity (MPI) estimates using the methodologies of Emanuel (1986, 1988, 1995a) and Holland (1997). CAPE as used here is defined following Williams and Renno (1993). Pseudoadiabatic ascent was assumed for an air parcel lifted from the lowest model level ($\sigma = 0.995$) using the ambient environmental relative humidity at the lowest model level; water condensate loading (Xu and Emanuel 1989), ice physics, and the convective inhibition energy contribution (Williams and Renno 1993) were not included. Emanuel's MPI method derives an estimate of the minimum possible central pressure based on the environmental temperature and moisture profiles and the SST. For the Emanuel MPI calculations in Fig. 7, we assume pseudoadiabatic, rather than reversible ascent, and neglect dissipative heating contributions. Holland's (1997) MPI method uses the environmental air temperature profile as input. The environmental state for each storm case in Fig. 7, was estimated from average conditions at the time of maximum intensity over a $10°$ longitude by $10°$ latitude storm-centered region, excluding the inner $5° \times 5°$ region (except for SST, where the inner region is included). This "outer box" estimate
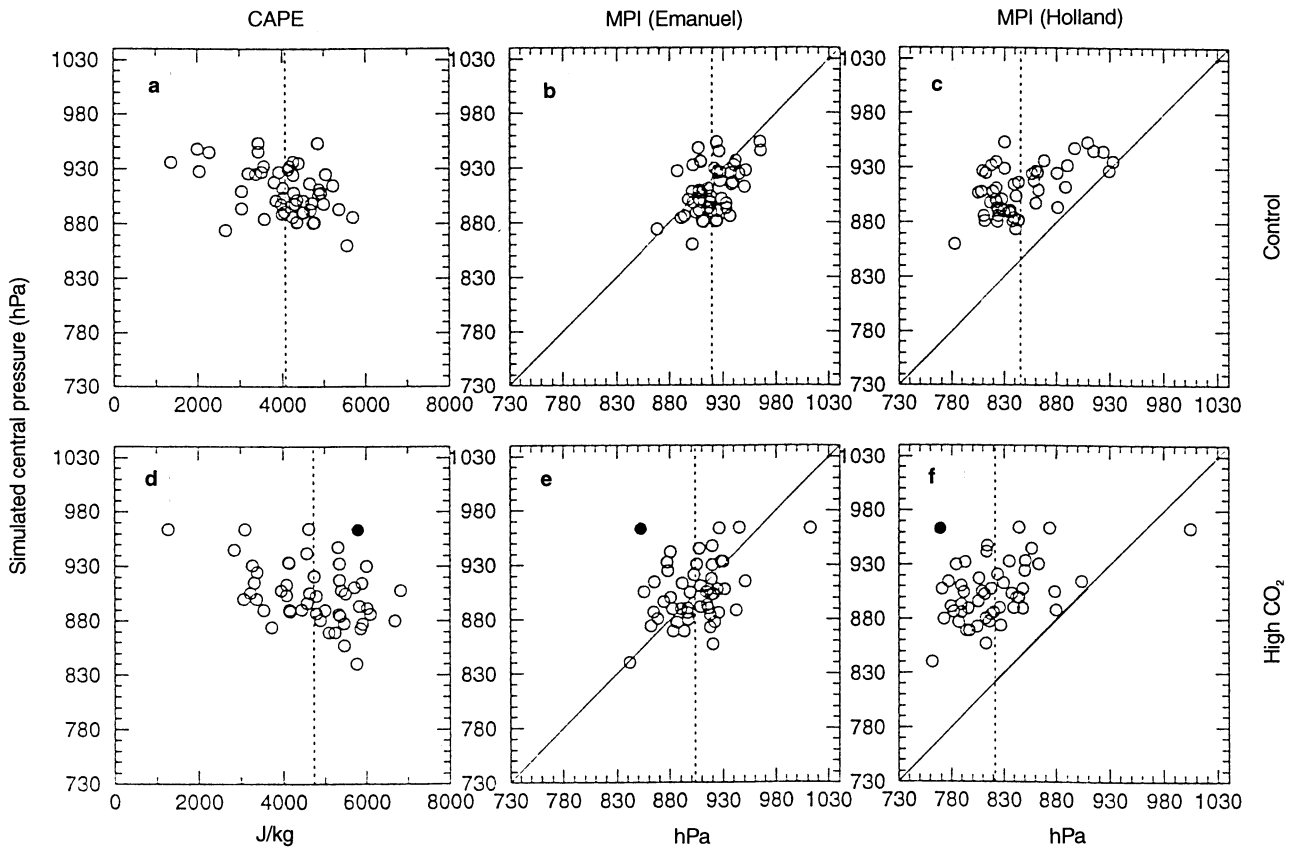
Fig. 7a–f Scatter plot of minimum surface pressure (hPa) versus environmental parameters as obtained from the hurricane model for 51 case studies each for **a–c** control and **d–f** high CO$_2$ conditions at the time of maximum intensity based on model fields sampled at 24-h intervals (see text for details). The environmental parameters are: CAPE in J/kg (**a, d**); Emanuel's MPI in hPa (**b, e**); or Holland's MPI in hPa (**c, f**). The *vertical dashed lines* show the mean CAPE or MPI values for the 51 cases. The *solid circles* in **d–f** denote an outlier case discussed in Sect. 4.4

was used in an effort to eliminate the storm's influence on the environmental state.

The dotted vertical lines in Fig. 7 depict the mean value for the abscissa, i.e., CAPE or MPI. The data indicate that the mean environmental CAPE value for the high CO$_2$ cases is about 16% greater than for the control. The mean CAPE for the control cases of about 4000 J/kg appears somewhat higher than the observed CAPE values for Ponape in the western Pacific (order 3000 J/kg) shown by Williams and Renno (1993). Both the Emanuel and Holland MPI methods indicate lower central pressures (higher upper-limit intensities) for the simulated high CO$_2$ environments than for the control. The mean MPI differences are 16 and 24 hPa for the Emanuel and Holland methods, which are also similar to the differences computed using the time-mean climate model profiles (10 and 18 hPa, respectively). Although the mean decrease in minimum central pressures for the model storms is only 4.2 mb, the mean simulated change is larger for the initialization method sensitivity experiments discussed in Sect. 4b (i.e., 16 hPa for the "no-bogus" experiments; and 22 hPa for the

weak bogus experiments). Thus our simulation results overall appear broadly consistent with the MPI calculations in terms of CO$_2$-induced intensity changes.

In addition to contrasting the high CO$_2$ and control environments, the results in Fig. 7 also show a fairly consistent relationship between variations of model intensity and variations of the CAPE and MPI within the samples. (An example of this type of comparison for observed Atlantic hurricanes is given by Emanuel 1995b.) Many of the simulated storms reached greater intensities than Emanuel's MPI (circles located beneath the diagonal line in Fig. 7b, e), although this is not the case with Holland's MPI (Fig.7c, f). In that regard, note that we neglected the effects of dissipative heating in applying Emanuel's method in an attempt to be more consistent with the hurricane model physical assumptions; including the dissipative heating term results in significantly more intense MPIs. Furthermore, we would not advocate comparing the actual magnitudes of the simulated intensities too literally with MPI theories, since our model's simulated intensities depend on many factors, such as model physics and resolution.

Table 1 Correlation between model simulated intensities (central surface pressure) and various environmental measures for area-averaged coditions surrounding the storm (as defined in the text) as of the time of minimum central pressure. Based upon case studies ($n = 51$) for both control and high CO_2 conditions. Absolute values larger than 0.23 are significantly different from zero at the 0.05 level, based on one-tailed tests of Student's distribution

Environmental measure	Control	High CO_2
SST	-0.58	-0.45
CAPE	-0.43	-0.39
Shear ($V_{856}-V_{223}$)	0.01	0.16
MPI (Emanuel, pseudoadiab.)	0.46	0.34
MPI (Holland)	0.58	0.41
CAPE (RH = 90%)	-0.59	-0.46

For this reason, we focus more on the correlation between simulated intensities and the MPIs or on relative changes in the values (high CO_2 versus control).

Table 1 summarizes the correlations for CAPE and the MPIs, along with similar intensity correlations based upon SST, windshear, and an alternative CAPE measure discussed below. The parameters analyzed are by no means an exhaustive list of factors that appear to contribute to storm intensification (e.g., Elsberry et al. 1992). For the control cases, the correlation with model intensity is -0.43 for CAPE; 0.46 for Emanuel's MPI and 0.58 for Holland's MPI. For the high CO_2 cases, these correlations are somewhat lower. The dark shaded circles in Fig. 7 on the three high CO_2 plots (Fig. 7d–f) highlight the results for a particular case in which a storm decayed despite a favorable thermodynamic environment (as estimated by MPI and CAPE) due to strong interaction with another storm. Without including this "outlier" case, to be discussed further in a later section, the correlations for the high CO_2 sample (-0.45, 0.45, 0.50) are fairly comparable to those for the control (Table 1). The correlation between SST and storm intensity in the model (Table 1) is comparable to that for CAPE or the MPI estimates.

To investigate the influence of environmental vertical wind shear, a different averaging procedure was adopted than for the other environmental factors. The storm-related wind fields were filtered from the storm region using the filtering process developed for operational bogusing and prediction with the hurricane model (Kurihara et al. 1993). The environmental shear was then defined as the magnitude of the vector difference between the filtered winds at $\sigma = 0.856$ and at $\sigma = 0.223$. The results show essentially no correlation between this wind shear measure and the model storm intensities (0.01 for the control and 0.16 for the high CO_2). A similar low correlation was obtained using other averaging areas, such as a $2°$ longitude $\times 2°$ latitude domain surrounding the storm center. As we will show later in this study (Sects. 4.4 and 5), there is a strong indication that hurricanes in our model

framework can be weakened at times by dynamical influences; nonetheless, a strong concurrent effect of windshear is not revealed in the above statistical analysis.

Results using an alternative CAPE measure (CAPE90) are also presented in Table 1. For CAPE90, which in fact is closely related to Holland's (1997) MPI, an environmental relative humidity of 90% is assumed for the location where the parcel ascent begins. The motivation for this measure is the assumption that the surface air temperature will be similar (isothermal) as one approaches the storm from the outer region, but that near the eyewall the surface relative humidity is greatly enhanced (to order 90%, following Holland 1997). Thus a parcel with initial relative humidity of 90% is more representative of what would occur in the eyewall region. Table 1 indicates that the CAPE90 has a somewhat higher correlation with simulated intensity than does CAPE.

Many of the environmental measures shown in Table 1 are significantly correlated with each other. For example, the correlation between SST and CAPE in our data is about 0.7; for SST versus CAPE90, the correlation rises to 0.9. The CAPE90 measure correlates with Holland's MPI at a level of 0.98 indicating the close relationship between these two measures.

4.3 Composite storm structure

The composite wind speed and temperature anomaly structures for the control and high CO_2 case studies are shown in Fig. 8. The composites are defined as the mean of all cases at the time of maximum intensity (from daily data) with all fields taken relative to the storm center (surface pressure minimum). For reference, the model's $1/6°$ inner nest covers an area extending out $2.5°$ from the center of the storm. The composite data are $1/3°$ interpolated data extending out $5°$ from the center. Figure 8 shows the longitude vs. pressure composite cross sections centered at the latitude of the storm. The wind speeds (Fig. 8a, b) are a maximum in the lower troposphere at a distance of about $2/3°$ (~ 70 km) from the storm center and show a pronounced decrease with height above the boundary layer. The warm core (Fig. 8d, e) increases in intensity with height, reaching a maximum at about 270 hPa in the control and at about 220 hPa (one model level higher) in the high CO_2 composite. The high CO_2 minus control wind speed difference field (Fig. 8c) shows a slight increase in wind speeds through the troposphere and a slight upward displacement of the height of the upper-level outflow in the high CO_2 composite. The upward shift of the warm core maximum is also clear from the temperature anomaly difference field (Fig. 8f). Thus, in terms of the overall storm size (high CO_2 versus control), there appears to be a slight but clearly detectable increase in the vertical
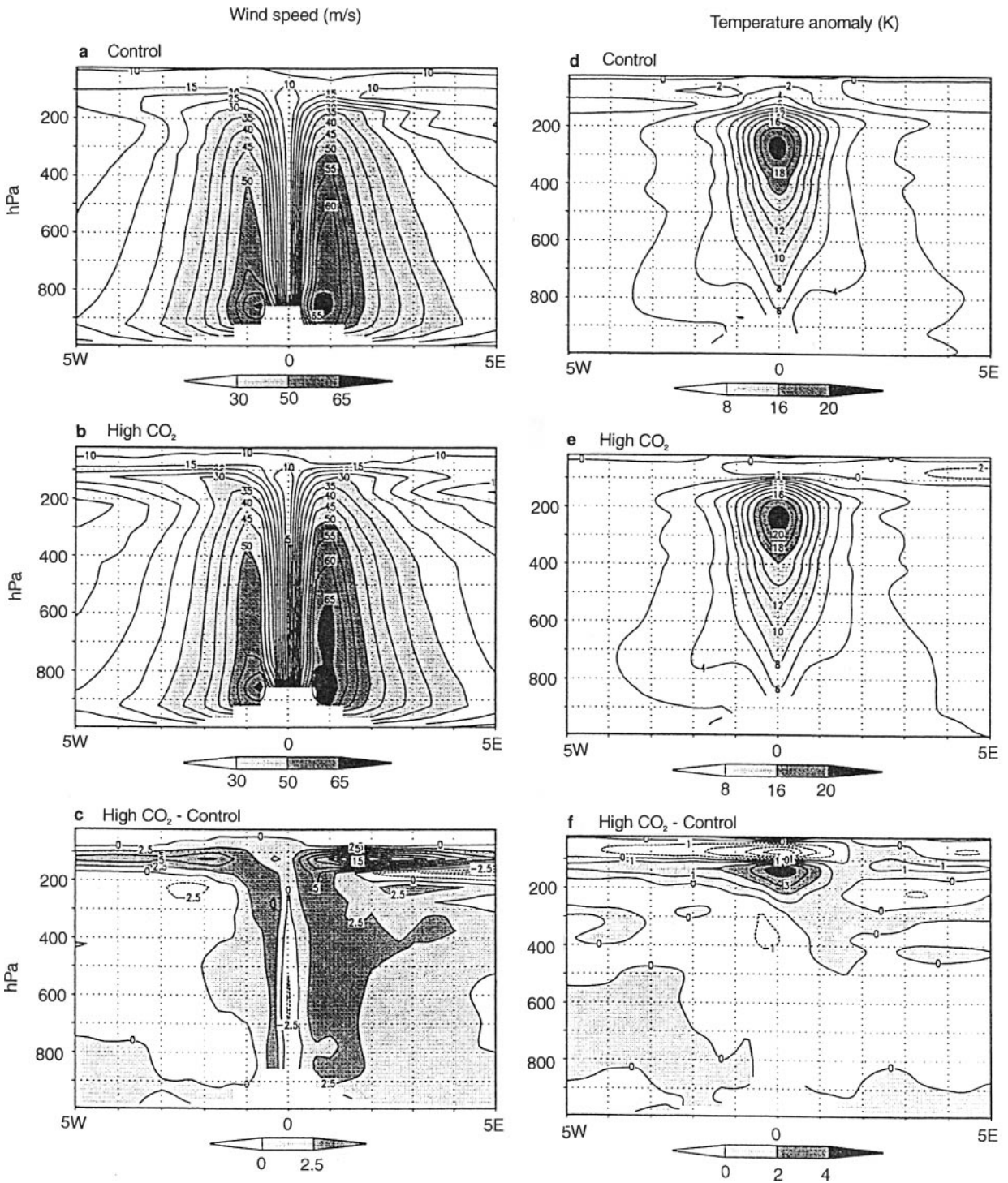
Fig. 8a–f Composite storm cross sections, relative to storm center, for **a, d** control and **b, e** high CO_2 cases, along with **c, f** their difference. The *left column* (**a–c**) shows wind speed in m/s, and the *right column* (**d–f**) shows temperature anomalies at each pressure level relative to the average over a $20° \times 20°$ domain centered on the storm

depth of the storm. However, the vertical resolution of the model, with sigma levels near the tropopause at $\sigma = 0.175$, 0.124, and 0.074, is probably not adequate for fully resolving this feature. A storm size parameter of greater relevance to storm-related damage than the

vertical depth is the mean horizontal radius of hurricane force winds, which increases slightly (by 2 to 3%) for the high CO_2 composite compared to the control.

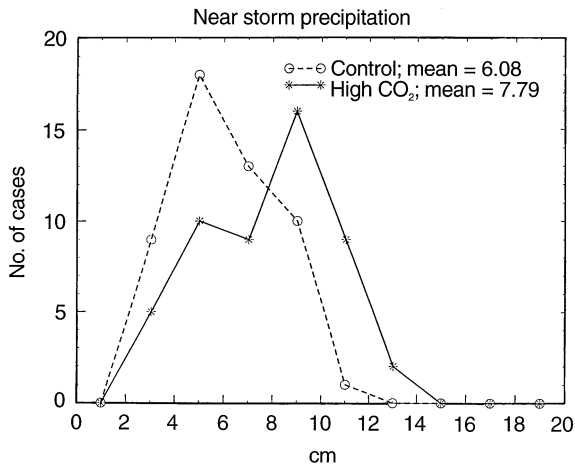A substantial increase in near-storm precipitation occurs with the high CO_2 storms. Figure 9 shows

Fig. 9 Frequency distribution of composite precipitation in the vicinity of the storm center (3.5°x3.5° region) for the control (*dashed curve*) and high CO_2 (*solid curve*) cases. The precipitation measure used is the six-hour accumulated precipitation as of the time of minimum central surface pressure

a histogram of near-storm precipitation values as of the time of maximum intensity for the control and high CO_2 samples. These are computed based on 6-h accumulated precipitation for a $3.5° \times 3.5°$ region in the vicinity of the storm center. The mean of the high CO_2 storm precipitation sample is 28% higher than for the control (7.79 cm versus 6.08 cm) and the two distributions are statistically distinct with $P = 0.0008$ according to a one-sided KS test. The 28% increase in near-storm precipitation is larger than the percentage increase in domain-averaged ($75° \times 75°$) evaporation and precipitation in the model over the 5-day experiments, both of which increase by about 10% in high CO_2 cases. The simulated precipitation increase is more statistically significant (and is a more easily detectable model signal) than the surface wind intensity increase, although as noted previously our results should be interpreted as applying only to the strongest storms. The simulated increase of hurricane-related precipitation is reminiscent of recent observational evidence (Karl and Knight 1998) of an upward trend in the intensity of extremely heavy precipitation events in the USA since 1910; however, their study did not distinguish between hurricane-related and other types of precipitation events.

4.4 A case of two interacting storms

As mentioned already, one of the cases is a particularly notable outlier in terms of its relatively weak intensity compared to its thermodynamic potential (e.g., MPI or CAPE). Maps of sea level pressure and upper troposphere ($\sigma = 0.175$) winds at 24-h intervals for this case are shown in Fig. 10. The initial disturbance (A) intensifies during the first 24 h. However, by hour 48 a second

storm (B) has formed to the west of storm A and is intensifying as well. Note that both A and B storms have well-defined upper-level divergent outflow at this time. By hour 72, the upper-level outflow from storm B appears to be crossing over the top of storm A, apparently causing storm A to weaken. (See also Merrill's 1988 composite upper tropospheric flow fields for observed non-intensifying hurricanes.) By hour 96 storm A has nearly dissipated as B continues to strengthen and moves off to the north during the fifth (final) day of the experiment. This case, along with the thermodynamic environment results in Fig. 7, strongly suggests that dynamical influences, such as storm inter-action, can at times play an overwhelming role in a simulated storm's evolution despite the presence of a highly favorable thermodynamic environment (Fig. 7) and a robust initial disturbance.

The strong degree of apparent interaction between the storms in Fig. 10 was unusual for our case studies, although some other cases showed some indication of storm interactions. As many as four distinct closed circulation systems appear at times in Fig. 10. In the real world, an occurrence of a succession of storms in the northwest Pacific has been discussed in some detail by Holland (1995) who noted that multiple storms can appear to form in association with a large-scale monsoon depression feature which organizes the large-scale flow in the region at times.
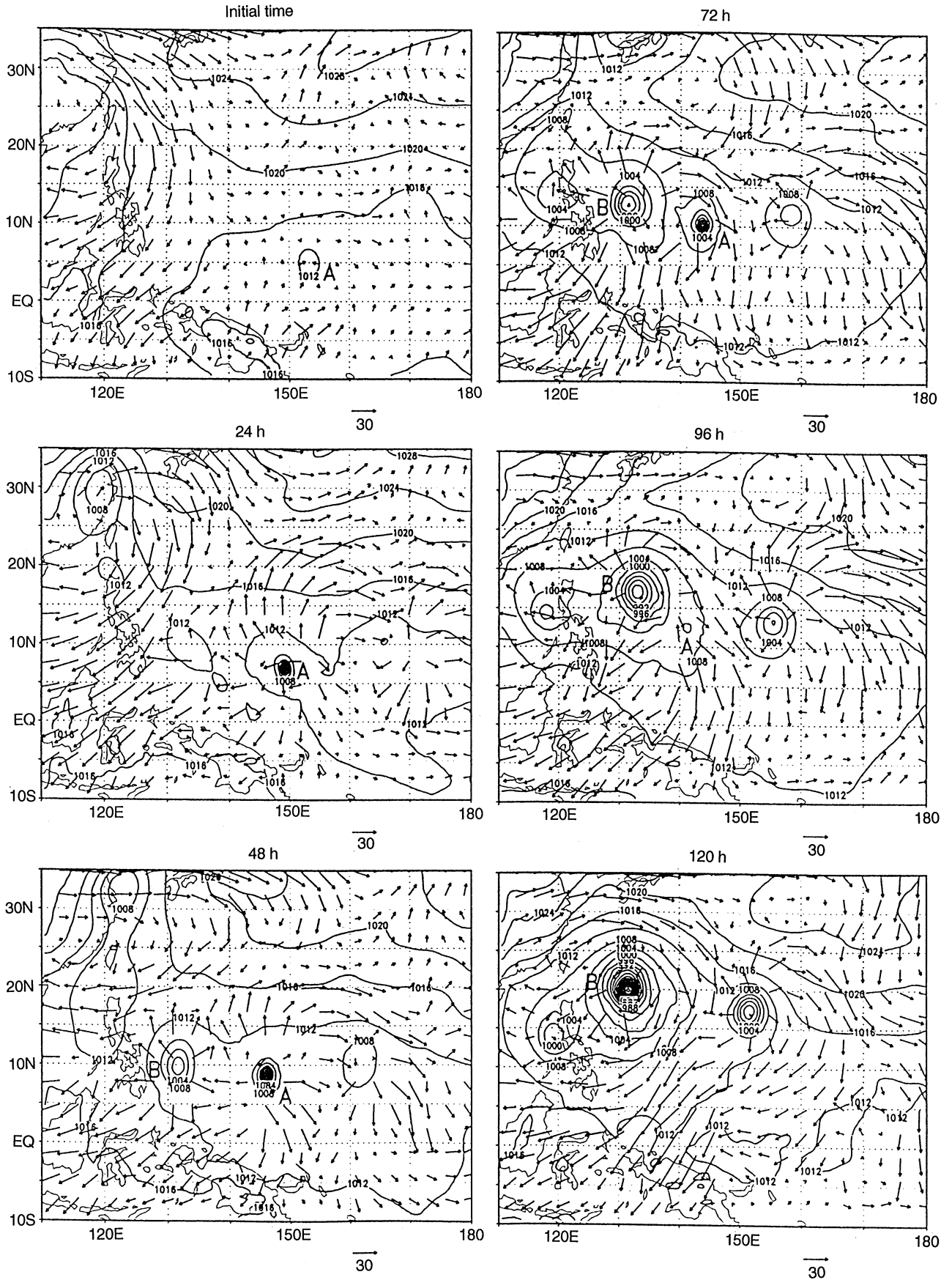
5 Idealized experiments

As an alternative to the case study approach, in this section the sensitivity of hurricane intensity to CO_2-induced changes in environmental conditions for different basins is explored using idealized environmental flow fields. This approach is used to help elucidate any CO_2-induced changes of intensity by reducing the "noise" due to synoptic variability of transient flow features that occurs in the case studies. On the other hand, the idealized flow fields are less realistic than those of the case studies.

5.1 Experimental design

The same triply nested version of the hurricane model is used as for the case studies. For each five-day

Fig. 10 Time sequence of sea level pressure (4 hPa contour interval) and upper level winds ($\sigma = 0.175$, see 30 m/s reference vector beneath each diagram) from a standard bogus case beginning October 9 of year 91 from the high CO_2 experiment. Maps depict conditions at 24-h intervals beginning with the initial time. *A* denotes the specified initial vortex and its subsequent evolution; *B* denotes a second storm which forms in the outer (1° resolution) mesh of the hurricane model

idealized experiment an initial disturbance is embedded in a highly simplified zonal flow with no other initial disturbances, no land, and approximately uniform SST (see later). The initial vortex was specified as in the standard case study experiments (i.e., 17.5 m/s maximum winds at a radius of 175 km) except that some perturbations were added as outlined later. The large-scale thermodynamic environments for the experiments were derived from the time-averaged, area-averaged SST, temperature, and water vapor fields from the climate model for each basin. For most of the cases, the environmental flow field was specified as a horizontally uniform 5 m/s easterly flow at all levels. Additional experiments were run for the NW Atlantic basin using the mean zonal wind profile (varying with height) from the climate model as the specified environmental flow. The surface pressure and the temperature fields are computed at the end of the vortex insertion procedure by solving a form of the reverse balance equation, using the climate model-derived temperatures as a reference boundary condition at the central latitude of the east-west channel. The temperature profiles at other latitudes along the boundaries could vary from the reference profile, for example, due to the presence of vertical wind shear in the NW Atlantic zonal wind profile experiments. The zonal means of SST away from the center of the channel were adjusted as necessary from the climate model-derived values in order to ensure a constant zonal mean environmental air-sea temperature difference. The CO_2 content in the hurricane model was increased by a factor of 2.57 above that of the control values for consistency with the mean conditions from the climate model, although sensitivity tests indicated that altering the CO_2 did not produce any statistically distinguishable effect beyond that obtained

by altering the environmental SSTs, air temperature, and moisture based on the climate model fields.

Preliminary results showed that even with the highly idealized environments, significant internal variability was present in the simulations. Therefore, we ran an ensemble of experiments (11 control and 11 high CO_2 cases) for each basin or environmental flow configuration considered. The individual elements of the ensembles differed only by small perturbations to the specified initial vortex intensity: specifically, the initial intensities were derived from a random Gaussian distribution with mean of 17.5 and standard deviation of 0.5 m/s.

5.2 Results of idealized experiments

The results from the idealized experiments are summarized in Fig. 11, which shows the statistical distributions of absolute minimum central surface pressures (hPa) for each series of idealized experiments. Each large circle represents the ensemble mean of the absolute minimum pressures obtained from a set of 11 idealized experiments for the basin indicated at the bottom of the diagram. Clear circles represent control cases, and solid circles represent high CO_2 cases. The column of ' + ' symbols indicate the lowest central surface pressures obtained for each individual element of the ensembles.

The results indicate a tendency for more intense storms under high CO_2 conditions for all of the basins. This tendency is highly statistically significant ($p_{KS} < 0.001$) for all basins except the South Indian, where the tendency is still significant, but p_{KS} is only 0.04. For the NW Pacific basin, the ensemble mean
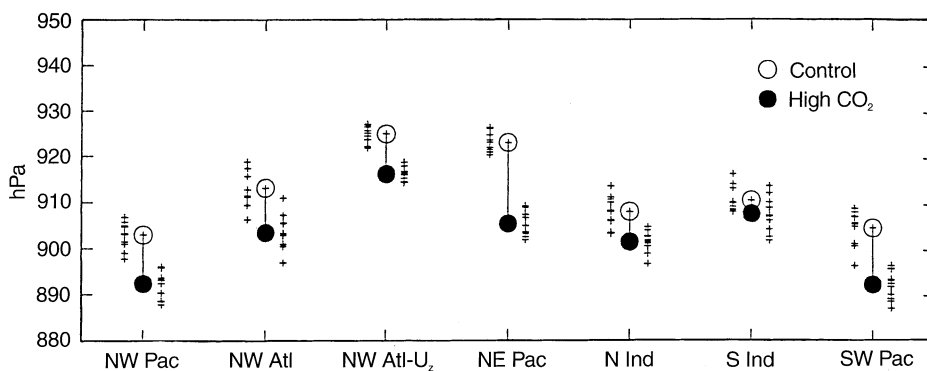

Fig. 11 Minimum central surface pressure statistics (hPa) for a series of idealized experiments. Each *large circle* represents the ensemble mean of the absolute minimum pressures obtained from a set of 11 idealized experiments for the basin indicated at the *bottom* of the *diagram*. *Clear circles* represent control cases, and *solid circles* represent high CO_2 cases. Each *small* ' + ' symbol represents the lowest central surface pressure obtained for an individual element of the ensemble of 5-day integrations. The control sample is displayed in a *column* to the *left* of the ensemble mean results, and the high CO_2 sample is to the *right*. The six tropical storm basins are defined in the captions to Figs. 2 and 3. For all cases, the wind field is specified to be a uniform easterly flow of 5 m/s except for the cases labeled "*NW Atl-Uz*" which use the mean zonal wind profiles from the global model for the NW Atlantic basin (see Fig. 2). See text for further details

difference in minimum central pressures (11 hPa) and the maximum wind speed increase (4.8%) are similar to that obtained using the case study approach with the standard initial bogus. The simulated CO_2-induced intensification in the other basins varies from 2.9 hPa lower central pressure and 2.9% increase in maximum wind speed in the South Indian basin to 18 hPa lower central pressure and 10% higher maximum wind speed in the NE Pacific basin. The larger response in the NE Pacific basin could be related to the slightly larger enhancement of lower tropospheric θ_e shown in Fig. 3b.

The NW Atlantic zonal wind profile cases (labelled "NW Atl-Uz" in Fig. 11) show the effect of a environmental flow field with substantial westerly shear (Fig. 2b). The intensities in these cases are reduced, compared to the uniform 5 m/sec easterly flow cases (i.e., "NW Atl"), for both control and high CO_2 conditions. This is consistent with observational evidence of the negative impact of vertical shear on tropical storm intensification (Gray 1968; DeMaria and Kaplan 1994b). Five-day time series of central pressures (not shown) from the NW Atlantic idealized experiments indicate that the negative impact of vertical shear on intensity is even more pronounced during the first two days of storm development than is indicated in Fig. 11, which is based on the minimum pressures achieved during the five-day simulations. The slight enhancement of vertical shear in the NW Atlantic basin in the high CO_2 climate (see Fig. 2b) does not appear to have a strong effect on the CO_2-induced intensification signal in these idealized experiments.

6 Discussion and conclusions

In this study, we have used the GFDL hurricane prediction system to explore the sensitivity of hurricane intensities to the changes in large-scale environmental conditions due to increasing CO_2 as simulated in the GFDL global climate model. The large-scale changes in environmental conditions can be characterized as a warming of about 2.2 °C for the sea surface and 2.5 °C in the lower troposphere, with a warming about twice as large (> 5 °C) in the upper troposphere. Relatively small changes in mean environmental relative humidity and wind shear are simulated in the global model. Given these environmental changes, the regional hurricane model simulates significantly stronger hurricane intensities in the high CO_2 environment. Surface wind speed increases of about 3–7 m/s (5–11%) and central surface pressure decreases of 7 to 24 hPa were simulated using a variety of initialization approaches for a series of NW Pacific basin case studies. The case study results are supported by more idealized experiments, which also suggest that the CO_2-induced storm intensification simulated for the NW Pacific basin is

qualitatively applicable to other tropical storm basins, at least in terms of the thermodynamic influences. However, since the case study approach has not yet been applied outside of the NW Pacific region, various dynamical influences such as transient disturbances or interannual deviations in vertical wind shear have not yet been assessed for the other basins. The latter effect is believed to be quite important for tropical storm activity in the NW Atlantic, for example through the remote dynamical influence of El Niño. The mean storm track for the high CO_2 case studies is quite similar to that for the control. The radius of hurricane force surface winds is about 2 to 3% larger for the high CO_2 composite storm, which also penetrates slightly higher into the upper troposphere than does the control. The simulated near-storm precipitation is about 28% greater in the high CO_2 sample than in the control, a result which may have important future societal consequences since precipitation from hurricanes can produce significant damage and fatalities in addition to that from the winds and storm surge at landfall.

Recently it has been suggested (Henderson-Sellers et al. 1998) that in a CO_2-warmed climate, any intensification of hurricanes due to increased SST would be moderated by the enhanced upper tropospheric warming such as that simulated in global climate model CO_2-increase experiments, where the tropical lapse rate remains close to moist adiabatic. Our idealized and case study results by design include this moderating effect. Despite the enhanced environmental dry stability, the large-scale environments in our high CO_2 experiments are less stable with regard to moist stability measures such as the vertical θ_e gradient and CAPE due to the large increase of lower tropospheric water vapor content. Thus, while the processes leading to more intense storms under high CO_2 conditions are not fully understood, the simulated increase of storm intensities in the present study appears consistent with the greater environmental evaporation rates, the higher potential intensities of storms as derived from the MPI theories of Emanuel and Holland, and the higher levels of environmental CAPE.

A notable feature of the present study is the relatively high resolution (∼18 km) used in the storm region as compared to previous investigations of hurricane intensity and greenhouse gas-induced warming. Some potentially important apparent effects of horizontal resolution were noted in the study. For example, the storm tracks for the cases from the global climate model appear to have a systematically more poleward trajectory than the tracks obtained using the high-resolution hurricane model. These results suggest that the use of coarse resolution global models may lead to poleward biases in storm trajectories, as well as lower than observed storm intensities and possibly lower sensitivity of storm intensities to climate warming as compared to higher resolution models.

Our case study results appear most applicable to the behavior of strong tropical cyclones (which are potentially the most damaging) as opposed to the mean intensity of all tropical storms. The tendency in our case studies to produce strong storms may be due in part to our neglect of ocean coupling effects. In that regard, it is worth noting that such ocean coupling effects depend strongly on details for each individual storm case, such as the ocean mixed-layer depth, which will vary temporally and geographically, and with the storm's translational speed. Future investigations of possible CO_2-induced changes in the near-surface ocean temperature structure would be useful for addressing this issue.

The 5–11% increase in the intensity of strong hurricanes simulated in the present study is in reasonable agreement with estimations based on theoretical MPI frameworks (Henderson-Sellers et al. 1998). Both the MPI methods (Emanuel 1987; Holland 1997) and our simulation approach (Knutson et al. 1998, Fig. 1) yield fairly realistic geographical distributions and magnitudes of the strongest hurricane intensities in the present climate. These results suggest that our methodology may provide a useful approximation to the actual sensitivity of strong hurricane intensities to a CO_2-induced global warming.

Appendix A. Criteria used to define a GCM tropical storm

The following criteria were used to identify candidate warm-core storms in the climate model simulation for use in the hurricane model case studies. The criteria are similar to those used in other recent GCM studies (e.g., Bengtsson et al. 1995).

1. Sea level pressure (SLP) local minimum with surface wind speed of at least 17.5 m/s at a point within a 5×5 gridpoint region surrounding the storm center.
2. Average surface rotational wind speed (V_ψ) of at least 8 m/s over a 5×5 region surrounding the storm center.
3. A total temperature anomaly, defined by $T'_{350} + T'_{500} + T'_{700}$ of at least 3 K, where ' is the deviation at the storm center from the average over a surrounding 7×7 point region.
4. The temperature anomaly increases with height: $T'_{350} > T'_{850}$.
5. The wind speed decreases with height: $WS_{850} > WS_{300}$, where wind speed is based on a 5×5 gridpoint region.

From the GCM storms meeting these criteria, the storm cases were selected from a pre-specified month and year (e.g., case 1 from July of year 120, case 2 from August of year 119, etc.). Storms from the months of July, August, September, October, and November were included in the ratio of 2:3:3:3:2, respectively, to mimic the seasonal cycle of tropical storm frequency in the NW Pacific. Candidate cases for the pre-specified month were examined in order of their intensity (strongest to weakest). To qualify as a case study, we required that a storm be traceable back in time for at least 48 hours prior to the time of maximum intensity (t_{max}) with at least one closed isobar (4 hPa contour) present 24 and 48 h prior to t_{max}. Such storms were traced back up to 96 h (4 days). The "initial time" for each case

study was designated as the earliest occurrence of a closed isobar or a maximum of 4 days prior to t_{max}. In about 10% of the years, no qualifying storm was found in the pre-specified month; in these cases, neighboring months were examined until the nearest (in time) qualifying case was found.

References

Baik J-J, Paek J-S (1998) A climatology of sea surface temperature and the maximum intensity of western North Pacific tropical cyclones. J Meteorol Soc Japan 76 : 129–137

Bender MA, Ginis I, Kurihara Y (1993) Numerical simulations of tropical cyclone-ocean interaction with a high-resolution coupled model. J Geophys Res 98**(**D12): 23 245–23 263

Bengtsson L, Botzet M, Esch M (1995) Hurricane type vortices in a general circulation model. Tellus 47 A : 175–196

Bengtsson L, Botzet M, Esch M (1996) Will greenhouse gas-induced warming over the next 50 years lead to higher frequency and greater intensity of hurricanes? Tellus 48 A : 57–73

Broccoli AJ, Manabe S (1990) Can existing climate models be used to study anthropogenic changes in tropical cyclone climate? Geophys Res Lett 17 : 1917–1920

Broccoli AJ, Manabe S (1992) Reply to Evans. Geophys Res Lett 19 : 1525–1526

Cunningham WM, Mitchell JFB (1990) On the dependence of climate sensitivity on convective parametrization. Clim Dyn 4 : 85–93

DeMaria M (1985) Tropical cyclone motion in a nondivergent barotropic model. Mon Weather Rev 113 : 1199–1210

DeMaria M, Kaplan J (1994a) Sea surface temperature and the maximum intensity of Atlantic tropical cyclones. J Clim 7 : 1324–1334

DeMaria M, Kaplan J (1994b) A statistical hurricane intensity prediction scheme (SHIPS) for the Atlantic basin. Weather Forecasting 9 : 209–220

Drury S, Evans JL (1993) Sea surface temperature and CAPE: importance for tropical cyclone intensity. Preprints, 20th Conf. on Hurricane and Tropical Meteorology, San Antonio, Am. Meteorol Soc., 89–92

Emanuel KA (1986) An air-sea interaction theory for tropical cyclones. Part I: Steady-state maintenance. J Atmos Sci 43 : 585–604

Emanuel KA (1987) The dependence of hurricane intensity on climate. Nature 326 : 483–485

Emanuel KA (1988) The maximum intensity of hurricanes. J Atmos Sci 45 : 1143–1155

Emanuel KA (1995a) Sensitivity of tropical cyclones to surface exchange coefficients and a revised steady-state model incorporating eye dynamics. J Atmos Sci 52 : 3969–3976

Emanuel KA (1995b) Comments on "Global climate change and tropical cyclones": Part I. Bull Am Meteorol Soc 76 : 2241–2243

Emanuel KA, Bister M (1996) Moist convective velocity and buoyancy scales. J Atmos Sci 53 : 3276–3285

Elsberry RL, Holland GJ, Gerrish H, DeMaria M, Guard C, Emanuel K (1992) Is there any hope to tropical cyclone intensity prediction? - A panel discussion. Bull Am Meteorol Soc 73 : 264–275

Evans JL (1993) Sensitivity of tropical cyclone intensity to sea surface temperature. J Clim 6 : 1133–1140

Evans JL, Ryan BF, McGregor JL (1994) A numerical exploration of the sensitivity of tropical cyclone rainfall intensity to sea surface temperature. J Clim 7 : 616–623

Fiorino M, Elsberry RL (1989) Some aspects of vortex structure related to tropical cyclone motion. J Atmos Sci 46 : 975–990

Gaffen DJ (1994) Temporal inhomogeneities in radiosonde temperature records. J Geophys Res 99 : 3667–3676

Gray WM (1968) Global view of the origin of tropical disturbances and storms. Mon Weather Rev 96 : 669–700

Haarsma RJ, Mitchell JFB, Senior CA (1993) Tropical disturbances in a GCM. Clim Dyn 8 : 247–257

Hansen J et al. (1997) Forcings and chaos in interannual to decadal climate change, J Geophys Res 102:25 679–25 720

Hamilton K, Hemler RS (1997) Appearance of a supertyphoon in a global climate model simulation. Bull Am Meteorol Soc 78:2874–2876

Henderson-Sellers A, Zhang H, Berz G, Emanuel K, Gray W, Landsea C, Holland G, Lighthill J, Shieh S-L, Webster P, McGuffie K (1998) Tropical cyclones and global climate change: a post-IPCC assessment. Bull Am Meteorol Soc 79:19–38

Holland GJ (1995) Scale interaction in the western Pacific monsoon. Meteorol Atmos Phys 56:57–79

Holland GJ (1997) The maximum potential intensity of tropical cyclones. J Atmos Sci 54:2519–2541

Kalnay E et al. (1996) The NCEP/NCAR 40-year reanalysis project. Bull Am Meteorol Soc 77:437–471

Karl TR, Knight RW (1998) Secular trends of precipitation amount, frequency, and intensity in the United States. Bull Am Meteorol Soc 79:231–241

Karoly DJ, Cohen JA, Meehl GA, Mitchell JFB, Oort AH, Stouffer RJ, Wetherald RT (1994) An example of fingerprint detection of greenhouse climate change. Clim Dyn 10:97–105

Kattenberg A et al. (1996) Climate models - projections of future change. In: Houghton JT et al. (eds) Climate change 1995: The science of climate change, Cambridge University Press, Cambridge, UK, 572 pp

Knutson TR, Manabe S (1998) Model assessment of decadal variability and trends in the tropical Pacific Ocean. J Clim 11:2273–2296

Knutson TR, Tuleya RE, Kurihara Y (1998) Simulated increase of hurricane intensities in a CO_2-warmed climate. Science 279:1018–1020

Krishnamurti TN, Correa-Torres R, Latif M, Daughenbaugh G (1998) The impact of current and possibly future sea surface temperature anomalies on the frequency of Atlantic hurricanes. Tellus 50 A:186–210

Kurihara Y, Bender MA, Ross RJ (1993) An initialization scheme of hurricane models by vortex specification. Mon Weather Rev 121:2030–2045

Kurihara Y, Tuleya RE, Bender MA (1998) The GFDL hurricane prediction system and its performance in the 1995 hurricane season. Mon Weather Rev 126:1306–1322

Kuroda M, Harada A, Tomine K (1998) Some aspects on sensitivity of typhoon intensity to sea-surface temperature. J Meteorol Soc Japan 76:145–151

Landsea CW, Nicholls N, Gray WM, Avila LA (1996) Downward trends in the frequency of intense Atlantic hurricanes during the past five decades. Geophys Res Lett 23:1697–1700

Levitus S (1982) Climatological atlas of the world ocean. NOAA Prof Pap 13, US Department of Commerce, Washington, DC, 173 pp

Luers JK, Eskridge RE (1998) Use of radiosonde temperature data in climate studies. J Clim 5:1002–1019

Manabe S, Stouffer RJ, Spelman MJ, Bryan K (1991) Transient response of a coupled ocean-atmosphere model to gradual changes of atmospheric CO_2. Part I: Annual mean response. J Clim 4:785–818

Merrill RE (1988) Environmental influences on hurricane intensification. J Atmos Sci 45:1678–1687

Ooyama K (1969) Numerical simulation of the life cycle of tropical cyclones. J Atmos Sci 26:3–40

Renno NO, Ingersoll AP (1996) Natural convection as a heat engine: a theory for CAPE. J Atmos Sci 53:572–585

Rotunno R, Emanuel KA (1987) An air-sea interaction theory for tropical cyclones. Part II: evolutionary study using a non-hydrostatic axisymmetric numerical model. J Atmos Sci 44:542–561

Royer JR, Chauvin F, Timbal B, Araspin P, Grimal D (1998) A GCM study of the impact of greenhouse gas increase on the frequency of occurrence of tropical cyclones. Clim Change 38:307–343

Siegel S, Castellan NJ (1988) Nonparametric statistics for the behavioral sciences 2nd edn. McGraw-Hill, New York

Tett SFB, Mitchell JFB, Parker DE, Allen MR (1996) Human influence on the atmospheric vertical temperature structure: detection and observations. Science 274:1170–1173

Tuleya RE, Kurihara Y (1982) A note on the sea surface temperature sensitivity of a numerical model of tropical storm genesis. Mon Weather Rev 110:2063–2069

Whitney LD, Hobgood JS (1997) The relationship between sea surface temperatures and maximum intensities of tropical cyclones in the eastern North Pacific Ocean. J Clim 10:2922–2930

Williams E, Renno N (1993) An analysis of the conditional instability of the tropical atmosphere, Mon Weather Rev 121:21–36

Xu K, Emanuel K (1989) Is the tropical atmosphere conditionally unstable? Mon Weather Rev 117:1471–1479